Supporting Information

Boron-catalyzed graphitized carbon coating in $Na_4Fe_3(PO_4)_2P_2O_7$ cathodes boosts reaction kinetics for high-rate and long-cycle sodium-ion batteries

Yuhan Xu[1], Jinbin Guo[1], Ningchun Li[2], Ling Chen[2], Yaoguo Fang[4], Qian Cheng[4], Haoxuan Zhang*[1,2], Hui Sun*[1,3], Hao Jiang*[1,2,3]

1. Shanghai Engineering Research Center of Hierarchical Nanomaterials, School of Chemical Engineering, East China University of Science and Technology, Shanghai 200237, China

2. Key Laboratory for Ultrafine Materials of Ministry of Education, School of Materials Science and Engineering, East China University of Science and Technology, Shanghai, 200237, China

3. Xinjiang Key Laboratory of Coal Clean Conversion & Chemical Engineering Process, School of Chemical Engineering, Xinjiang University, Urumqi, 830046, Xinjiang, China

4. Shanghai Xuanyi New Energy Development Co., Ltd, Shanghai 201800, China

1. Figures

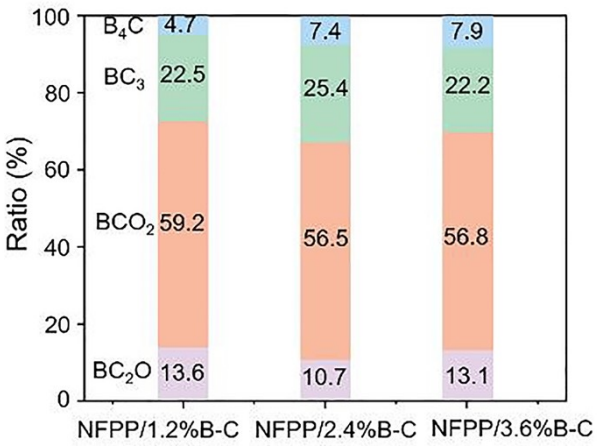

Figure S1. The content of B_4C, BC_3, BCO_2 and BC_2O in NFPP/1.2%B-C, NFPP/2.4%B-C and NFPP/3.6%B-C.

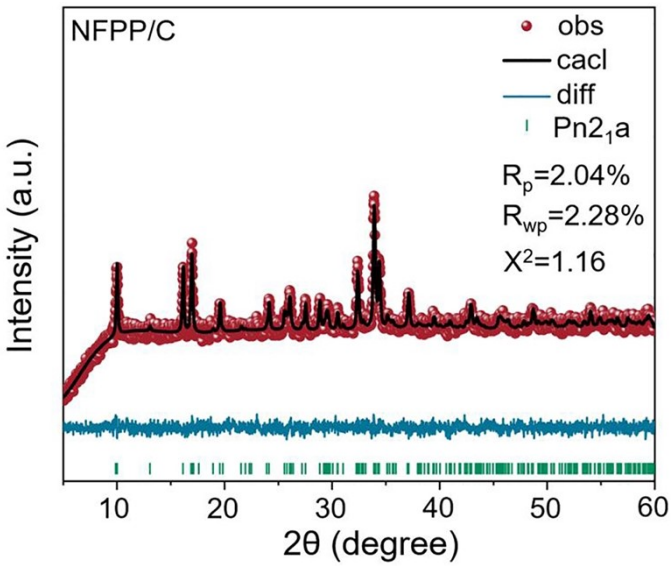

Figure S2. XRD Rietveld refinement result of NFPP/C.

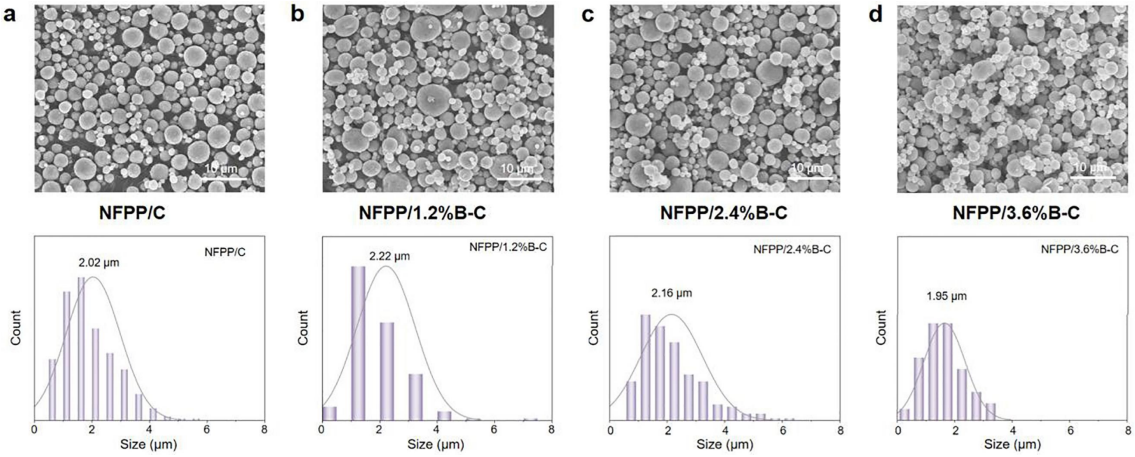

Figure S3. SEM images of the secondary particles and average particle size of (a) NFPP/C, (b) NFPP/1.2%B-C, (c) NFPP/2.4%B-C and (d) NFPP/3.6%B-C.

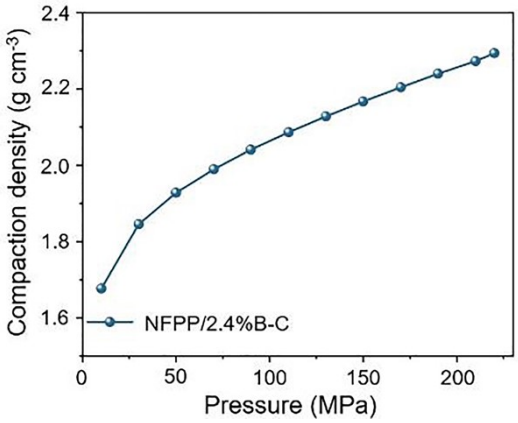

Figure S4. The compaction density of NFPP/2.4%B-C under different pressure.

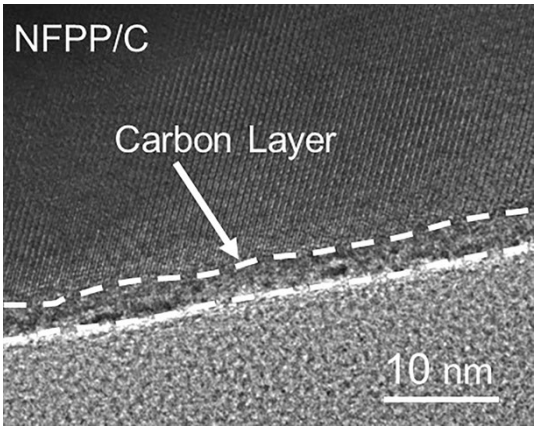

Figure S5. High-resolution TEM image of NFPP/C.

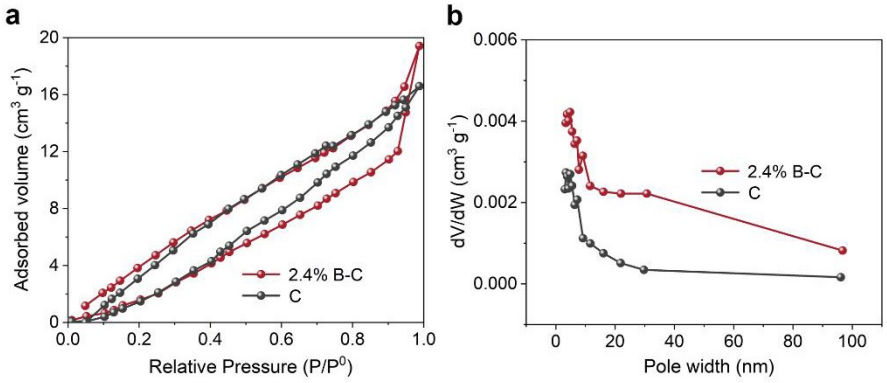

Figure S6 Nitrogen adsorption-desorption isotherms and pore size distribution of C and 2.4%B-C.

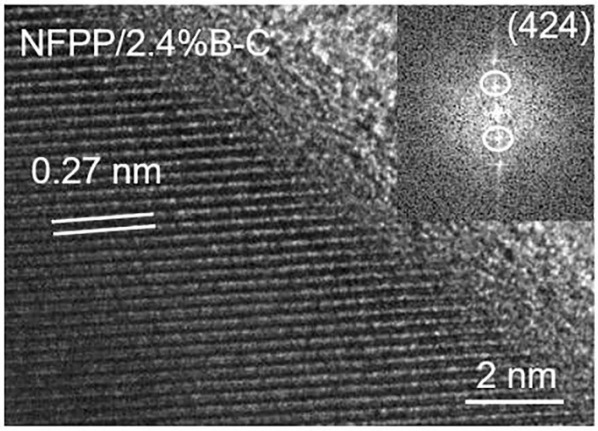

Figure S7. High-resolution TEM image of NFPP/2.4% B-C.

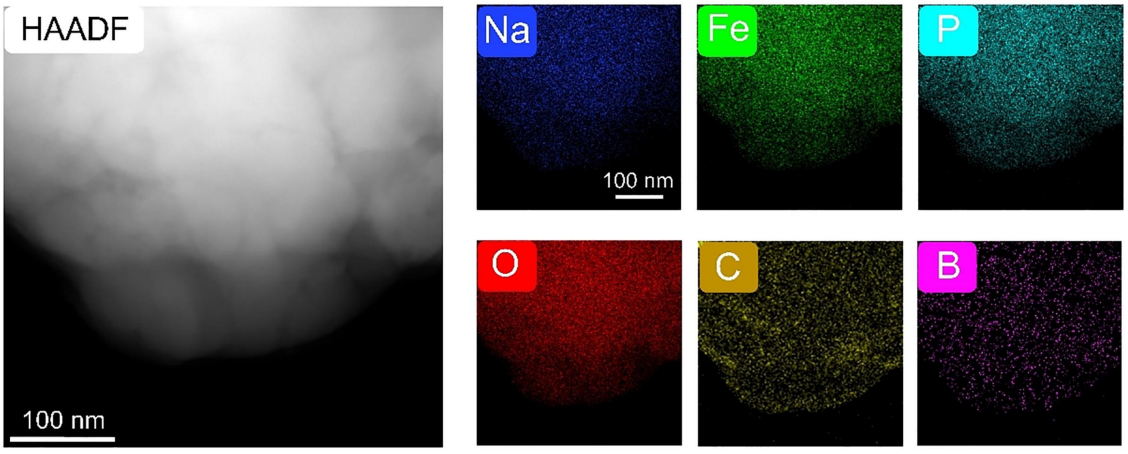

Figure S8. HAADF TEM of EDS maps of NFPP/2.4%B-C.

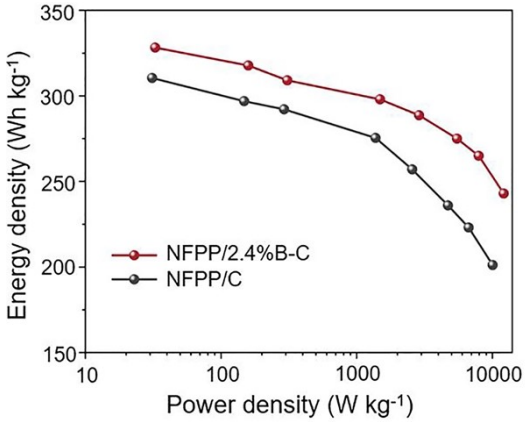

Figure S9. Energy density vs power density of NFPP/C and NFPP/2.4%B-C.

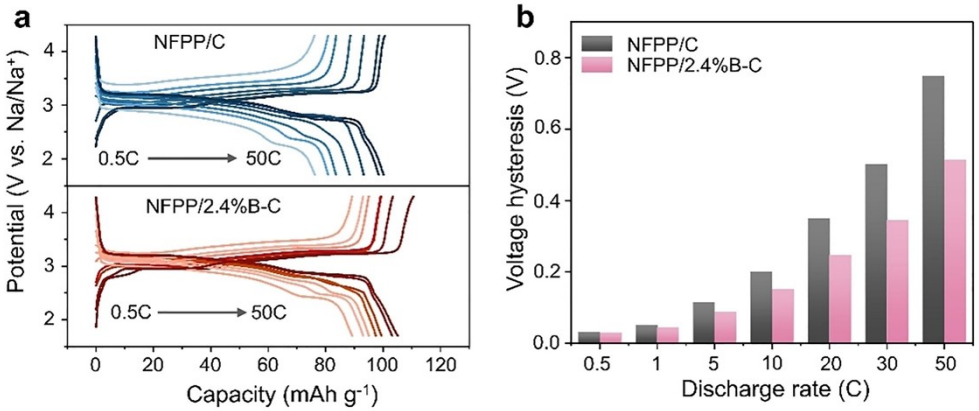

Figure S10. (a) Charge/discharge voltage profiles and (b) voltage hysteresis of NFPP/C and NFPP/2.4%B-C electrodes at different current rates.

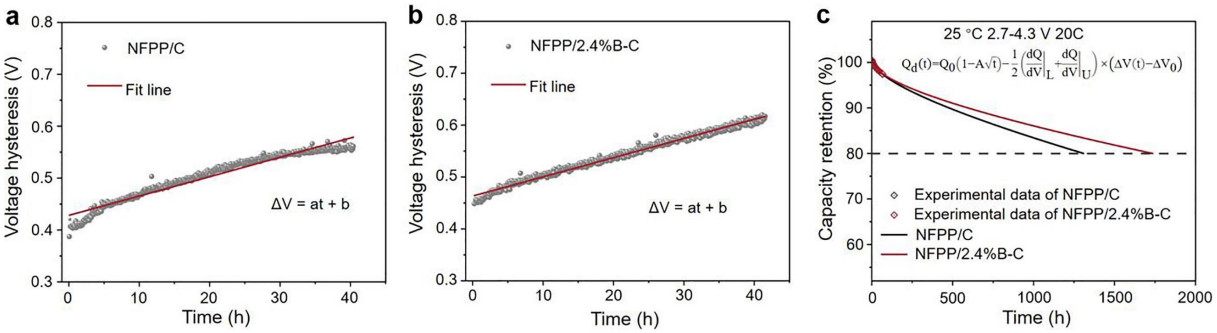

Figure S11. (a,b) The linear fitting of voltage hysteresis *vs*. time. (c) The fitting curves of capacity decay *vs*. time within 2.7-4.3 V at 20C.

Through inputting the data from 715 cycles at 20C for both NFPP/2.4%B-C and NFPP/C into this model, the real-time capacity $Q_d(t)$ over the cycle time (t) for NFPP/2.4%B-C can be expressed as follows:

$$Qd(t) = 98.43 \times (1-0.00228\sqrt{t}) - 0.00334 \times t$$

And the final equation for NFPP/C can be expressed as follows:

$$Qd(t) = 89.37 \times (1-0.00373\sqrt{t}) - 0.00491 \times t$$

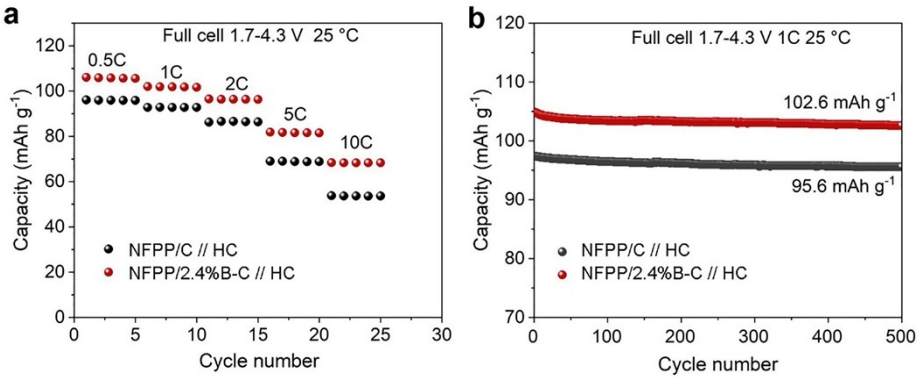

Figure S12. Coin-type full-cell performance of NFPP/C and NFPP/2.4%B-C.

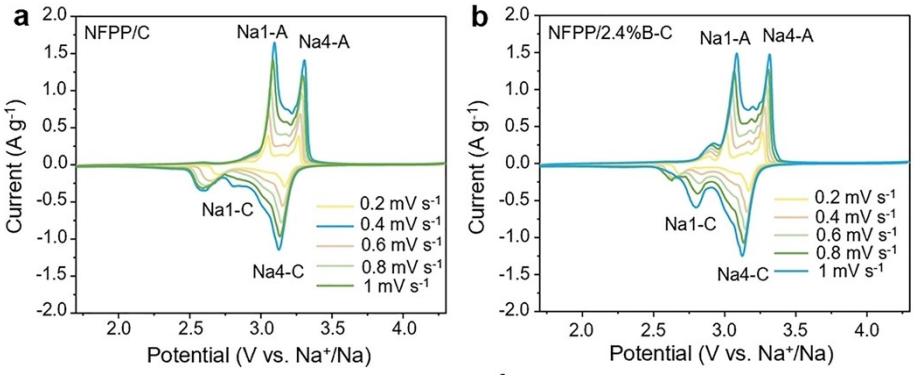

Figure S13. CV curves under different current densities of (a) NFPP/C and (b) NFPP/2.4%B-C.

2. Tables

Table S1 The atomic composition of the NFPP/C and NFPP/2.4%B-C.

Sample	C (%)	B (%)	O (%)
C surface	87.43	/	12.57
C subsurface	88.82	/	11.18
2.4%B-C surface	84.91	0.87	14.22
2.4%B-C subsurface	87.68	1.79	10.52

Table S2 XRD Rietveld refinement results of the NFPP/C and NFPP/2.4%B-C.

Sample	Lattice parameters			
	a(Å)	b(Å)	c(Å)	V(Å^3)
NFPP/C	18.110	6.534	10.646	1259.74
NFPP/2.4%B-C	18.119	6.542	10.632	1260.23